PHYSICAL REVIEW B **79**, 165434 (2009)

Propagating, evanescent, and localized states in carbon nanotube–graphene junctions

J. González,[1] F. Guinea,[2] and J. Herrero[1]
[1]*Instituto de Estructura de la Materia, Consejo Superior de Investigaciones Científicas, Serrano 123, 28006 Madrid, Spain*
[2]*Instituto de Ciencia de Materiales de Madrid, Consejo Superior de Investigaciones Científicas, Cantoblanco, 28049 Madrid, Spain*
(Received 21 January 2009; published 27 April 2009)

We study the electronic structure of the junctions between a single graphene layer and carbon nanotubes, using a tight-binding model and the continuum theory based on Dirac fermion fields. The latter provides a unified description of different lattice structures with curvature, which is always localized at six heptagonal carbon rings around each junction. When these are evenly spaced, we find that it is possible to curve the planar lattice into armchair $(6n,6n)$ as well as zigzag $(6n,0)$ nanotubes. We show that the junctions fall into two different classes, regarding the low-energy electronic behavior. One of them, constituted by the junctions made of the armchair nanotubes and the zigzag $(6n,0)$ geometries when n is a multiple of 3, is characterized by the presence of two quasibound states at the Fermi level, which are absent for the rest of the zigzag nanotubes. These states, localized at the junction, are shown to arise from the effective gauge flux induced by the heptagonal carbon rings, which has a direct reflection in the local density of states around the junction. Furthermore, we also analyze the band structure of the arrays of junctions, finding out that they can also be classified into two different groups according to the low-energy behavior. In this regard, the arrays made of armchair and $(6n,0)$ nanotubes with n equal to a multiple of 3 are characterized by the presence of a series of flat bands, whose number grows with the length of the nanotubes. We show that such flat bands have their origin in the formation of states confined to the nanotubes, with little overlap in the region between the junctions. This is explained in the continuum theory from the possibility of forming standing waves in the mentioned nanotube geometries, as a superposition of modes with opposite momenta and the same quantum numbers under the C_{6v} symmetry of the junction.

DOI: 10.1103/PhysRevB.79.165434 PACS number(s): 81.05.Uw, 73.22.−f, 73.63.−b, 73.23.−b

I. INTRODUCTION

The recent isolation of graphene layers a single atom thick[1–3] has led to a great deal of activity, because of their novel electronic properties and potential applications. The lattice structure of graphene is determined by the sp^2 coordination between neighboring carbon atoms. Each carbon atom has three nearest neighbors, leading to planar honeycomb lattice. With small modifications, the same structure describes other carbon allotropes, such as the fullerenes and the carbon nanotubes.

In this paper we study the simplest systems which combine two of these allotropes: the junctions between a single graphene layer and carbon nanotubes. A regular array of closely spaced armchair nanotubes attached to a graphene layer has already been studied,[4] and related systems are being considered for their potential applications.[5] We undertake here the investigation of junctions made of nanotubes with different chiralities, which have in common a transition from the planar to the tubular geometry mediated by the presence of six heptagonal carbon rings. These induce the negative curvature needed to bend the honeycomb carbon lattice at the junction, playing a kind of dual role to that of the pentagonal carbon rings in the fullerene cages.[6]

We analyze first the electronic properties of a single junction between a carbon nanotube and a graphene layer. We discuss the possible structures of this type, concentrating on geometries where the heptagonal rings are evenly spaced around the junction. The nanotubes can be then either armchair $(6n,6n)$ or zigzag with $(6n,0)$ geometry (that is, with $6n$ hexagonal rings around the tube). We calculate their electronic structure, using the tight-binding model based on the π orbitals of the carbon atoms widely applied to carbon allotropes with sp^2 coordination.

Paying attention to the local density of states, we find that the junctions fall into two different classes, depending on the behavior in the low-energy regime. One of the classes, comprising the junctions made of armchair and $(6n,0)$ nanotubes when n is a multiple of 3, is characterized by the presence of a peak in the density of states close to the Fermi level. The peak is absent in the other class, formed by the junctions made with the rest of zigzag geometries. In general, the density of states tends to be depleted in the junction at low energies, with peaks above and below the Fermi level marking the threshold for the propagation of new states across the junction.

We present next a continuum description, based on the formulation of Dirac fermion fields in the curved geometry, which allows us to characterize the general properties of the junction, and which is consistent with the previous discrete analysis. Thus, we see that the peak at the Fermi level in the local density of states is in general a reflection of the existence of quasibound states (zero modes) for the Dirac equation in the curved space of the junction. It is known that the topological defects of the honeycomb lattice (pentagonal and heptagonal rings) induce an effective gauge field in the space of the two Dirac points of the planar graphene lattice.[7] It turns out that the effective magnetic flux is enough to localize two states at the junctions made of armchair or $(6n,0)$ nanotubes when n is a multiple of 3. At low energies, however, the generic behavior is given by evanescent states, which arise from the matching of modes with nonvanishing

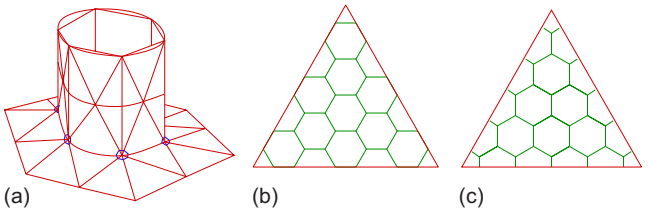

FIG. 1. (Color online) (a) Sketch of carbon nanotube attached to a graphene plane. The building blocks of the structure are triangles which include many carbon atoms. The orientation of the bonds of the honeycomb lattice in the basic triangle may give rise to (b) armchair or (c) zigzag nanotubes. The threefold coordination of the carbon atoms induces the existence of six heptagonal rings, schematically shown in blue at the corners of the hexagonal prism contacting the plane in (a).

angular momentum and have exponential decay in the nanotube.

We finally apply our computational framework to the analysis of the band structure of the arrays of nanotube-graphene junctions. Considering the behavior of the low-energy bands close to the Fermi level, we find that the arrays also fall into two different classes. The arrays made of armchair nanotubes or $(6n,0)$ nanotubes with n equal to a multiple of 3 tend to have a series of flat bands close to the Fermi level, while the arrays made with the rest of zigzag nanotubes have all the bands dispersing at low energies. Such a different behavior has its origin in the existence of states confined in the nanotube side of the junction. We find that this feature can also be explained in the context of the continuum model. The armchair and the $(6n,0)$ geometries with n equal to a multiple of 3 allow for the formation of standing waves between the junction and the other end of the tube. This is the mechanism responsible for the confinement of the states in the nanotubes and the consequent development of the flat bands, whose number grows at low energies with the length of the nanotube, in agreement with the predictions of the continuum theory.

II. TIGHT-BINDING APPROACH TO CARBON NANOTUBE-GRAPHENE STRUCTURES

A. Lattice structure

Our first aim is to analyze the density of states of a semi-infinite nanotube attached to a graphene layer in the tight-binding approximation. The possible setups that we will consider, keeping the threefold coordination of the carbon atoms, are sketched in Fig. 1. The structures can be wrapped by the graphene hexagonal lattice, with the exception of the six points where the sides of the hexagonal prism (which describes the nanotube) intersect the plane. The threefold coordination of the carbon atoms requires the existence of sevenfold rings at those positions.

We describe the electronic states in the structures shown in Fig. 1 by means of a nearest-neighbor tight-binding model. In general the relaxation of elastic energy will modify the bond lengths at the junction, depending on the nanotube radius. We will assume that this relaxation does not change significantly the electronic behavior. In this respect, a tight-binding model based on the π carbon orbitals is well suited for the purpose of discerning the extended or localized character of the different electronic states. Our main achievement will be to assign the different features in the local density of states to the behavior of the electronic states near the nanotube-graphene junctions. To this aim, we have actually checked that slight modulations of the transfer integral t near the junctions do not produce significant changes in the results shown in what follows.

B. Electronic densities of states

We concentrate on the analysis of geometries where the six heptagonal carbon rings are evenly spaced around the junction as in Fig. 1. This constrains the possible chiralities of the nanotubes, that can be then either armchair $(6n,6n)$ or zigzag $(6n,0)$, with the number n running over all the integers. Nanotubes in which the carbon sheet is wrapped with helicity can be also attached at the expense of introducing an irregular distribution of the heptagonal rings. Anyhow, we expect that the rules explaining the different features in the density of states are universal enough to hold even in these more general cases.

We have obtained the spectra of different types of hybrid structures by diagonalization of the tight-binding Hamiltonian for very large lattices, with up to $\approx 50\,000$ carbon atoms in the graphene part and $\approx 40\,000$ in the nanotube side. Given that the whole geometry has C_{6v} symmetry, we have classified the energy eigenstates into six groups according to the eigenvalue q under a rotation of $\pi/3$. The nature of each electronic state is given in general by its behavior at the nanotube-graphene junction. For this reason, we have characterized the hybrid structures in terms of the local density of states averaged over a circular ring of atoms at the end of the nanotube close to the junction.

Our computations have covered a number of structures including armchair and zigzag nanotubes with different radii. After inspection of all the spectra, it becomes clear that there are several generic features in the density of states. We have represented in Fig. 2 the behavior near the junction between a graphene layer and a (54,0) zigzag nanotube. We observe that, apart from the peak close to zero energy in the sectors corresponding to $q=e^{\pm i\pi/3}$, for $q\neq 1$ there is always a depletion in the density of states at low energies, delimited by two abrupt upturns. It is remarkable that the pattern in the sectors corresponding to $q=e^{\pm 2i\pi/3}$ reproduces the same observed for $q=e^{\pm i\pi/3}$, but with a scale that is approximately twice larger. The density of states in the sector with $q=-1$ displays in turn a wider depletion, with the position of the peaks scaled by an approximate factor of 3 with respect to those in the $q=e^{\pm i\pi/3}$ sectors.

In the above behavior of the density of states, the appearance of the peak close to zero in the sectors with $q=e^{\pm i\pi/3}$ is the only feature not generic for all kinds of nanotubes. In the junctions made with zigzag nanotubes, the peak actually appears for nanotube geometries of the type $(6n,0)$ when n is a multiple of 3. In this series of hybrid structures, the patterns in the density of states for each value of q are quite similar,

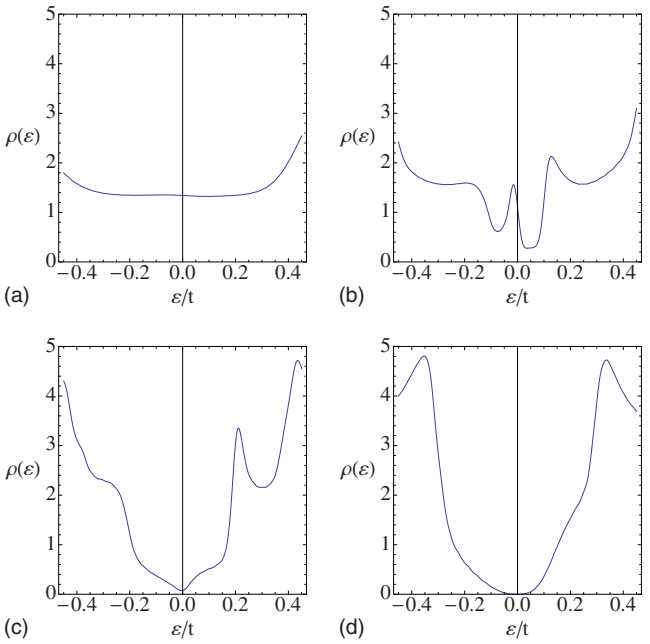

FIG. 2. (Color online) Sequence of local densities of states for a circular ring of atoms at the end of a (54,0) nanotube close to the junction, for the different sectors corresponding to eigenvalue q under $\pi/3$ rotation equal to (a) 1, (b) $e^{\pm i\pi/3}$, (c) $e^{\pm 2i\pi/3}$, and (d) -1. Energy is measured in units of the transfer integral t.

with the position of the corresponding peaks scaled in inverse proportion to the radius of the nanotube. On the other hand, the rest of junctions, for which n is not a multiple of 3, display a different behavior. We have represented in Fig. 3 the local density of states averaged over a ring of atoms at the end of a (48,0) nanotube close to the junction. It can be observed the depletion of the density of states at low energies

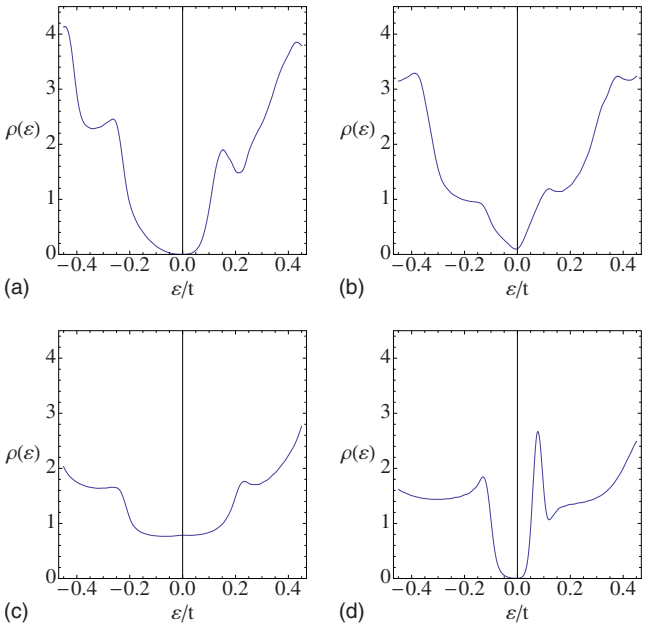

FIG. 3. (Color online) Similar sequence as in Fig. 2 for a (48,0) nanotube close to the junction, for (a) $q=1$, (b) $e^{\pm i\pi/3}$, (c) $e^{\pm 2i\pi/3}$, and (d) -1.

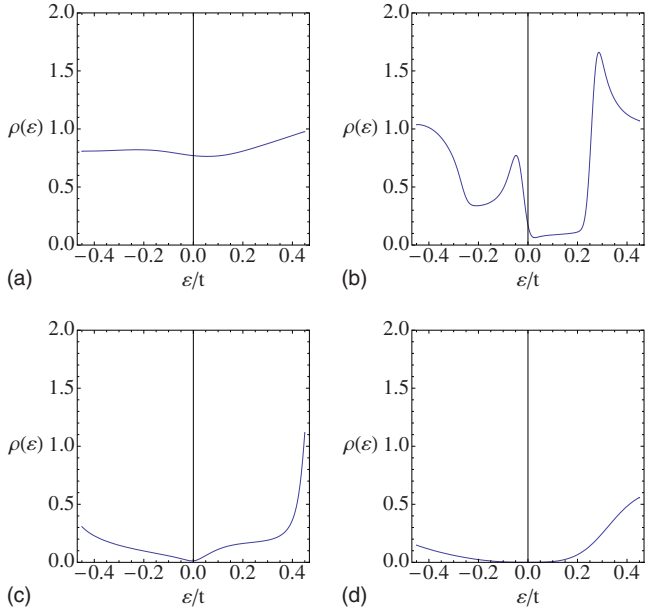

FIG. 4. (Color online) Similar sequence as in Fig. 2 for a (12,12) nanotube close to the junction, for (a) $q=1$, (b) $e^{\pm i\pi/3}$, (c) $e^{\pm 2i\pi/3}$, and (d) -1.

in all but one of the q-sectors, and the absence of a peak at zero energy in any of the sectors.

The local density of states of the (48,0) nanotube is dominated at the junction by contributions from states with $q=e^{\pm 2i\pi/3}$, and this has to do with the fact that the lowest-energy subbands of a $(6n,0)$ zigzag nanotube have a nonvanishing angular momentum equal to $\pm 4n$ for the motion around the tubule.[8] This corresponds to a quantum number $q=e^{\pm 2i\pi/3}$ in the case of the (48,0) nanotube, while the low-energy states have $q=1$ in the (54,0) nanotube. The present picture becomes then consistent with the fact that states in higher subbands may propagate across the junction only above (or below) some threshold energy. This feature will be established more precisely in the continuum approach derived below in terms of the Dirac equation.

At this point, the hybrid structures can be classified into two different groups, depending on whether there is a peak or not close to zero energy in the local density of states around the nanotube-graphene junction. The peak comes actually from the contribution of a doubly degenerated level with states having $q=e^{\pm i\pi/3}$, and whose probability distribution decays exponentially in the nanotube. The character of these states will be established in Sec. III, after developing the continuum limit in terms of Dirac fermion fields.

The evidence for the two different classes of hybrid structures is reinforced by the fact that the junctions made with armchair nanotubes behave in a quite similar way to that shown by the $(6n,0)$ nanotubes when n is a multiple of 3. The local density of states averaged over a circular ring of atoms around the junction between a (12,12) nanotube and a graphene layer has been represented in Fig. 4. We observe the presence of the peak close to zero energy in the sectors with $q=e^{\pm i\pi/3}$. There is a clear depletion in the local density of states at low energies except in the sector with $q=1$, which is consistent with the fact that the lowest-energy sub-

bands in the armchair nanotube correspond to zero angular momentum around the tubule.

The existence of the two different classes of nanotube-graphene junctions is illustrated in Fig. 5, which shows the results for the local density of states around the junction (after summing over the sectors with different values of q) for the different types of nanotube considered above. It is remarkable the similarity between the density of states for the (18,0) and (12,12) nanotube geometries, which have a very close value of the radius. This suggests that there must be a universal way of understanding the low-energy electronic properties of the two different classes of junctions, independent of the details of the lattice building the junction within each class.

III. CONTINUUM APPROACH

A. Heptagonal rings, effective flux, and matching at the junction

We observe that the density of states summed over all values of q tends to have an approximate linear behavior away from the very low energy regime. This motivates the analysis of the junction in terms of the Dirac equation in the hybrid geometry, as the Dirac fermions provide an appropriate description of the electronic properties in the one-dimensional (1D) carbon nanotube as well as in the two-dimensional (2D) graphene layer.

We will then assume that the radius R_0 of the nanotube is much larger than the graphene lattice constant, in order to obtain the continuum limit of the tight-binding model. Within this approximation, the analysis of the electronic structure is reduced to the study of the Dirac equation in a space with an abrupt change from a planar to a cylindrical structure. The transition from a geometry to the other takes place due to the presence of the six heptagonal rings at the junction. These defects are the source of negative curvature, playing a role opposite to that of the pentagonal rings in a fullerene cage.[6]

The heptagons, as well as the pentagons, also induce frustration in the honeycomb lattice, and lead to the exchange of the two Dirac valleys of the planar geometry.[7] This latter effect has to be accounted for by means of an effective non-Abelian gauge field operating in the space of the two independent Dirac points of graphene. It can be shown that the effective flux associated to an individual heptagonal ring is equal to $\pi/2$ (Ref. 7) (in units such that $\hbar=1$). The flux provided by the six heptagons at the junction can reach therefore a maximum of 3/2 times the flux quantum. In general, however, the count of the total flux may not follow an additive rule, so that it can be lower than the maximum value, depending on the relative position of the heptagonal rings.[9] We will see that this is actually the origin of the two different classes of junctions.

Note that the angular momentum around the axis of the nanotube is conserved and quantized in integer units, in a continuum description of the geometry analyzed here. On the other hand, the angular momentum in the plane is quantized and shifted by 1/2 plus the number of flux quanta of the effective gauge field induced by the heptagonal rings. The existence of topological defects which induce an effective flux at the junction allows us to match wave functions with different angular momenta at either side of the junction, provided that the effective flux corresponds to a half-integer number of quanta.

B. Continuum wave functions

By looking at the effect of pairs of heptagonal rings, the non-Abelian gauge field operating in the space of the two Dirac points becomes anyhow proportional to a sigma matrix τ_3. We may consider then that the effect of the six heptagonal rings at the junction is described by an effective Abelian field, standing for either of the eigenvalues of τ_3.[7] We end up therefore with two different Dirac equations, with effective magnetic fluxes of opposite sign. By denoting the Dirac spinors satisfying the two Dirac equations as Ψ^+ and Ψ^-, we can write them in the region of the plane with radius $r \geq R_0$,

$$iv_F \boldsymbol{\sigma} \cdot (\boldsymbol{\nabla} \mp ie\mathbf{A})\Psi^{\pm} = \varepsilon \Psi^{\pm}, \tag{1}$$

where v_F is the Fermi velocity and $\mathbf{A}$ is the vector potential corresponding to a number g of quanta of effective flux felt by the electrons when making a complete tour around the junction. In order to match the spinor wave functions at $r=R_0$ with those from the nanotube side, it is convenient to use polar coordinates r, θ, for which $eA_r=0$, $eA_\theta=g$. In the above equation, $\boldsymbol{\nabla}$ is a covariant derivative which in curvilinear coordinates includes the spin connection $\boldsymbol{\Gamma}$, so that $\boldsymbol{\nabla}=\boldsymbol{\partial}+\boldsymbol{\Gamma}$.[10] In polar coordinates we have $\Gamma_r=0$, $\Gamma_\theta=-i\sigma_3/2$, and the Dirac equations for $r \geq R_0$ take finally the form,

$$iv_F\left(\partial_r + \frac{i\partial_\theta}{r} \pm \frac{g}{r} + \frac{1}{2r}\right)\Psi_A^{\pm}(r,\theta) = \varepsilon \Psi_B^{\pm}(r,\theta), \tag{2}$$

$$iv_F\left(\partial_r - \frac{i\partial_\theta}{r} \mp \frac{g}{r} + \frac{1}{2r}\right)\Psi_B^{\pm}(r,\theta) = \varepsilon \Psi_A^{\pm}(r,\theta), \tag{3}$$

where Ψ_A and Ψ_B denote the respective amplitudes of the electron in the two sublattices of the graphene lattice.

In the nanotube side, we use cylindrical coordinates z, θ, with $z \leq 0$. The Dirac equation for the nanotube is

$$iv_F\left(\partial_z + \frac{i\partial_\theta}{R_0}\right)\Psi_A^{\pm}(z,\theta) = \varepsilon \Psi_B^{\pm}(z,\theta), \tag{4}$$

$$iv_F\left(\partial_z - \frac{i\partial_\theta}{R_0}\right)\Psi_B^{\pm}(z,\theta) = \varepsilon \Psi_A^{\pm}(z,\theta). \tag{5}$$

We observe that the form of the Dirac equations in this part of the space does not depend on the effective magnetic flux, as the electrons turning around the nanotube cannot feel the effect of the heptagonal rings placed at the junction.

We note that Eqs. (2) and (3) as well as Eqs. (4) and (5) are expressions of the Dirac equation in flat space. This is consistent with the fact that, in the continuum limit, the curvature is localized at the circle connecting graphene and the nanotube. As an alternative to the coordinate z, we could make for instance the change in variables $r=R_0 \exp(z/R_0)$,

allowing us to map the nanotube into the region of the plane with $r<R_0$. Using a common radial coordinate $r>0$ to describe both graphene and the nanotube, the metric of the space turns out to be multiplied by the conformal factor $\Omega(r)=\theta(r-R_0)+(R_0/r)^2\theta(R_0-r)$. The first derivative of the metric becomes then discontinuous and the curvature scalar, computed in terms of second derivatives of the metric, is $R=-2r\delta(r-R_0)$. The integral of this expression corresponds actually to the total curvature provided by the heptagonal rings. This makes clear that the effects of the curvature are implicit in the operation of matching the solutions of Eqs. (2) and (3) and Eqs. (4) and (5) at the circle $r=R_0$.

The solutions of the Eqs. (2) and (3) are of the form

$$\begin{pmatrix} \Psi_A^{\pm}(r,\theta) \\ \Psi_B^{\pm}(r,\theta) \end{pmatrix} \equiv c_1 \begin{pmatrix} J_{n\mp g-1/2}(kr) \\ -i\ \mathrm{sgn}(\varepsilon) J_{n\mp g+1/2}(kr) \end{pmatrix} e^{in\theta} + c_2 \begin{pmatrix} Y_{n\mp g-1/2}(kr) \\ -i\ \mathrm{sgn}(\varepsilon) Y_{n\mp g+1/2}(kr) \end{pmatrix} e^{in\theta}, \quad (6)$$

where c_1 and c_2 are constants, and $J_n(x)$ and $Y_n(x)$ are Bessel functions. The energy is $\varepsilon=\pm v_F k$.

On the other hand, the resolution of Eqs. (4) and (5) shows that there are propagating and evanescent waves in the nanotube, which can be written as

$$\begin{pmatrix} \Psi_A^{\pm}(z,\theta) \\ \Psi_B^{\pm}(z,\theta) \end{pmatrix} \equiv \begin{cases} c_1' \begin{pmatrix} 1 \\ -\mathrm{sgn}(\varepsilon) e^{i\phi(k)} \end{pmatrix} e^{ikz} e^{in\theta} + c_2' \begin{pmatrix} 1 \\ \mathrm{sgn}(\varepsilon) e^{-i\phi(k)} \end{pmatrix} e^{-ikz} e^{in\theta} & |\varepsilon| > \dfrac{v_F|n|}{R_0} \\ c \begin{pmatrix} 1 \\ -\mathrm{sgn}(\varepsilon) e^{i\phi(-i\kappa)} \end{pmatrix} e^{\kappa z} e^{in\theta} & |\varepsilon| \le \dfrac{v_F|n|}{R_0}, \end{cases} \quad (7)$$

where c_1', c_2', and c are constants, the energy ε is given by

$$\varepsilon = \begin{cases} \pm v_F \sqrt{k^2 + \dfrac{n^2}{R_0^2}}, & |\varepsilon| > \dfrac{v_F|n|}{R_0} \\ \pm v_F \sqrt{-\kappa^2 + \dfrac{n^2}{R_0^2}}, & |\varepsilon| \le \dfrac{v_F|n|}{R_0}, \end{cases} \quad (8)$$

and the phase factor in Eq. (7) is:

$$e^{i\phi(k)} = \frac{k + \dfrac{in}{R_0}}{\sqrt{k^2 + \dfrac{n^2}{R_0^2}}} \quad (9)$$

We note that the evanescent states with longitudinal decay $e^{\kappa z}$ arise for nonvanishing angular momentum n. Then there is an energy threshold $v_F|n|/R_0$ for the appearance of propagating states in the nanotube. This is perfectly consistent with the behavior of the local density of states obtained for the different values of q in the tight-binding approach. The depletion found in different q sectors for the local density of states at the end of the nanotube (close to the junction) corresponds actually to the range of evanescent states given by Eq. (8). As already mentioned, the position of the peaks delimiting the depletion in the tight-binding approach scales in proportion to the value of the angular momentum, which corresponds in the lattice to the different values of q. Moreover, we have also seen that such a position is inversely proportional to the nanotube radius R_0, with values in the plots that can be approximately matched with the estimate $v_F n/R_0$ (after using the expression of the Fermi velocity $v_F=3ta/2$, in terms of the transfer integral t and the C-C distance a). We find therefore that the generic features found for the local density of states in the tight-binding approach are well captured by the continuum limit based on the Dirac equation.

C. Zero-energy states

The presence of a peak in the local density of states close to zero energy (in the sectors $q=e^{\pm i\pi/3}$) is the only feature not generic for all types of nanotubes, and that can be also explained within our continuum approach. The rotation caused by each heptagonal ring in the space of the two Dirac points corresponds to an effective magnetic flux of $\pi/2$,[7] but the way this flux is combined in the case of pairs of heptagons depends on their relative position. This has been studied in the case of pentagon pairs in Ref. 9, arriving at a conclusion that can be readily generalized to the case of heptagonal defects. The result is that, when the distance between the heptagons is given by a vector (N,M) (using the same notation to classify the nanotubes) such that $N-M$ is not a multiple of 3, the effective flux of a pair of heptagons does not add to π, but to the lower amount $\pi/3$. The number $N-M$ for the distance between heptagons is a multiple of 3 only in the case of junctions with armchair nanotubes, or with $(6n,0)$ nanotubes when n is a multiple of 3. In these instances, the total flux felt around the junction is equal to the sum of the fluxes provided by the individual heptagons, giving a value of $g=3/2$. In the rest of the cases, the total flux corresponds instead to $g=1/2$.

The number g of flux quanta has a direct correspondence with the number of zero modes of the Dirac equation. Their existence rests on the possibility of having localized states at

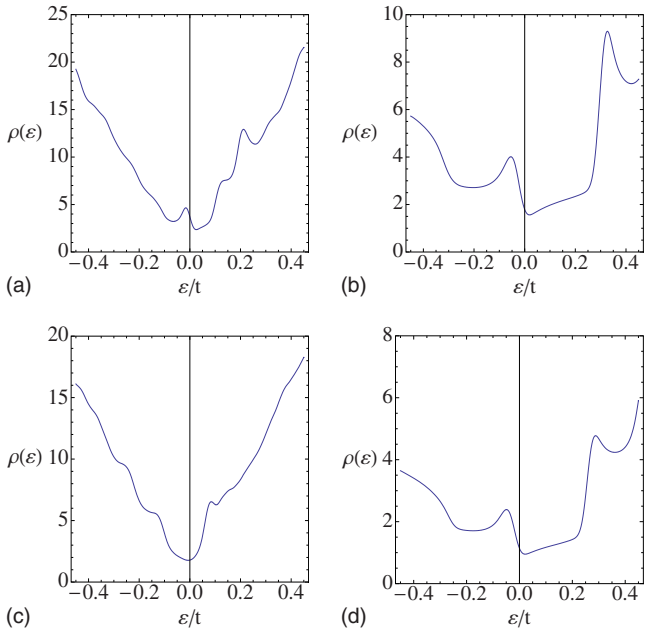

FIG. 5. (Color online) Sequence of local densities of states for a ring of atoms at the end of the nanotube close to the junction, for the different geometries (a) (54,0), (b) (18,0), (c) (48,0), and (d) (12,12). Energy is measured in units of the transfer integral t.

the junction, with suitable decay in both the graphene part and the nanotube side. If we take for instance the maximum effective flux and $g=3/2$, we have an equation for a zero-energy eigenstate in the region $r>R_0$,

$$\left(\partial_r + \frac{i\partial_\theta}{r} + \frac{2}{r}\right)\Psi_A(r,\theta) = 0. \tag{10}$$

For a wave function with angular momentum n, we obtain the behavior,

$$\Psi_A(r,\theta) \sim r^{n-2}e^{in\theta}. \tag{11}$$

This gives rise to modes decaying from the junction for values $n \leq 1$. The wave function has to be matched at $r=R_0$ with the appropriate dependence in the nanotube, that is

$$\Psi_A(z,\theta) \sim e^{(n/R_0)z}e^{in\theta}. \tag{12}$$

Recalling that $z \leq 0$, we see that only the value $n=1$ provides a localized state at the junction. On the graphene side, the state is not strictly normalizable, in a similar way to other half-bound states induced by defects.[11,12] Anyhow, such a localized state has a reflection in the peak observed close to zero energy in the $q=e^{\pm i\pi/3}$ sectors of the tight-binding density of states. By inverting the direction of the flux and taking $g=-3/2$, it can be seen that the solutions have then a nonvanishing component $\Psi_B(r,\theta)$ similar to Eq. (11), but with angular momentum $-n$ instead of n. Another localized state is found therefore with opposite chirality and $n=-1$.

In the case of the junctions with $(6n,0)$ nanotubes such that n is not a multiple of 3, the flux corresponding to $g=1/2$ is not enough to localize states at the junction. It can be seen that there are no zero-energy solutions of the Dirac equation decaying simultaneously in the graphene plane and in the nanotube. This explains why in this type of junctions there is no low-energy peak within the depleted region of the local density of states. We complete in this way the correspondence between the tight-binding approach and the continuum limit based on the Dirac equation, accounting for the main electronic features and unveiling also the origin of the different low-energy behavior in the two classes of junctions.

D. Transmission into the nanotube

Equations (6) and (7) allow us to analyze the scattering of a wave in the plane off the nanotube. We define transmission as the propagation of an electron from the graphene layer into the nanotube. The removal of particles from the layer can be viewed as an inelastic scattering process,[13] which leads to the loss of phase coherence of the wave function of the layer.

The coefficients c_1, c_2, c_1', and c_2' define the transmission and reflection by the nanotube. For a wave coming from the plane, the coefficient c_2' is zero, and c_1' is proportional to the transmission coefficient. Using the theory of scattering of two-dimensional Dirac electrons by an impurity,[14–18] the transmission coefficient is given by

$$T_n = \sqrt{\frac{\pi kR_0}{2}}\frac{iJ_{n+1}(kR_0)Y_n(kR_0) - iJ_n(kR_0)Y_{n+1}(kR_0)}{iY_n(kR_0) - Y_{n+1}(kR_0)e^{i\phi(k)}}. \tag{13}$$

At high energies, $\epsilon \gg v_F/R_0$ or, alternatively, $kR_0 \to \infty$, we can use the asymptotic expansion,

$$\lim_{kR_0\to\infty} J_n(kR_0) \approx \sqrt{\frac{2}{\pi kR_0}}\cos\left(kR_0 - \frac{n\pi}{2} - \frac{\pi}{4}\right),$$

$$\lim_{kR_0\to\infty} Y_n(kR_0) \approx \sqrt{\frac{2}{\pi kR_0}}\sin\left(kR_0 - \frac{n\pi}{2} - \frac{\pi}{4}\right), \tag{14}$$

and $\lim_{kR_0\to\infty} e^{i\phi(k)} = 1$. From these expansions, we obtain

$$\lim_{kR_0\to\infty} T_n \approx \frac{i}{i\sin\left(kR_0 - \frac{n\pi}{2} - \frac{\pi}{4}\right) + \cos\left(kR_0 - \frac{n\pi}{2} - \frac{\pi}{4}\right)e^{i\phi(k)}} \to e^{i[kR_0 - (n\pi/2) - (\pi/4)]} \tag{15}$$

so that $\lim_{kR_0\to\infty}|T_n|^2=1$. This estimate is valid for angular momenta n such that $n\ll kR_0$. We can also obtain the reflection coefficient in this limit, $\bar{R}_n$, which is also independent of n for $n\ll kR_0$. The angular dependence of the scattering cross section $\sigma(\theta)$ is

$$\sigma(\theta)\propto R_0\frac{\sin(kR_0\theta/2)}{\sin(\theta/2)}, \tag{16}$$

and the total transport cross section, $\sigma_{\rm tr}=\int_{-\pi}^{\pi}\sigma(\theta)[1-\cos(\theta)]d\theta$, is proportional to k^{-1} (see also Ref. 19). The total flux of particles propagating inside the nanotube, normalized to the total incoming flux, goes as $\sigma'=\int_{-\pi}^{\pi}\sigma(\theta)d\theta$, and it is proportional to R_0.

In the low energy limit, $kR_0\ll 1$, we obtain

$$\lim_{kR_0\to 0}|T_n|^2\approx\begin{cases}0, & kR_0\le n-1\\ \dfrac{\pi}{n!^2}\left(\dfrac{kR_0}{2}\right)^{2n+1}, & kR_0>n-1,\end{cases} \tag{17}$$

In this limit, most of the electrons reaching the junction are scattered back into the plane.

We consider here the nanotube to be semi-infinite. In this case, the only structures in the density of states of the nanotube are the Van Hove singularities at the edges of the subbands. We expect resonances in the transmission coefficient at these energies.

The knowledge of the total scattering cross section, $\sigma_{\rm tr}$, allows us to obtain the mean-free path, $l_{\rm tr}$, of electrons in the graphene layer in the presence of a random distribution of nanotubes with concentration $n_{\rm nt}$, $l_{\rm tr}\sim 1/(\sigma_{\rm tr}n_{\rm nt})$. The dependence of the graphene conductivity on the electron wave vector k_F is (see also Ref. 19)

$$\sigma\approx\frac{e^2}{h}k_F l_{\rm tr}\propto\frac{e^2}{h}\times\begin{cases}\dfrac{1}{n_{\rm nt}R_0^2}, & k_FR_0\ll 1,\\ \dfrac{k_F^2}{n_{\rm nt}}, & k_FR_0\gg 1\end{cases} \tag{18}$$

E. Local density of states

We can make use of the continuum equations to analyze systems of very large sizes. We calculate the electronic Green's functions numerically. The Dirac equation in the plane, in radial coordinates, can be discretized.[20] Each radial equation can be approximated by a nearest-neighbor tight-binding model with two inequivalent hoppings,

$$t\left(1+\frac{2n+1}{4i}\right)a_i+t\left(1-\frac{2n+1}{4i}\right)a_{i+1}=\epsilon b_i,$$

$$t\left(1+\frac{2n+1}{4i}\right)b_{i-1}+t\left(1-\frac{2n+1}{4i}\right)b_i=\epsilon a_i, \tag{19}$$

where a_i and b_i give the values of $\Psi_A^n(r)$ and $\Psi_B^n(r)$ at position $r=i\times a$, a being a length scale which defines the discretization. Equation (19) also include an energy scale, t, which plays the role of an upper cutoff. The Fermi velocity is equal to $t\times a$. The Dirac equation is obtained for $\epsilon\ll t$. We can write Eq. (19) in a more compact form using a single index, c_i, such that $c_{2j-1}=a_j$ and $c_{2j}=b_j$, so that

$$t_ic_{i-1}+t_{i+1}c_{i+1}=\epsilon c_i, \tag{20}$$

where, using as new length scale $a/2$, we have

$$t_i=t\left[1-(-1)^i\frac{2n+1}{4(i+N_0)}\right], \tag{21}$$

where we start at position N_0. The diagonal Green's function at site i can be written as

$$\mathcal{G}_{ii}(\epsilon)=\frac{1}{\epsilon-t_iT_+^i-t_{i+1}T_-^{i+1}}, \tag{22}$$

and

$$T_+^{i+1}=\frac{t_{i+1}}{\epsilon-t_iT_+^i},$$

$$T_-^i=\frac{t_i}{\epsilon-t_{i+1}T_-^{i+1}}, \tag{23}$$

with boundary conditions at $i=0$ and $i=N$,

$$T_+^0=\frac{1}{\epsilon-\Sigma_0(\epsilon)},$$

$$T_-^N=\frac{1}{\epsilon-\Sigma_N(\epsilon)}, \tag{24}$$

and

$$\Sigma_0(\epsilon)=\frac{t^2\left(1+\dfrac{n-1}{2N_0}\right)^2}{\epsilon}+\frac{\tilde{\epsilon}}{2}-\frac{\sqrt{\tilde{\epsilon}^2-4\tilde{t}^2}}{2},$$

$$\Sigma_N(\epsilon)=it, \tag{25}$$

and

$$\tilde{\epsilon}=\epsilon-\frac{t^2}{\epsilon}\left(1+\frac{(n-1)^2}{4N_0^2}\right),$$

$$\tilde{t}=\frac{t^2}{\epsilon}\left(1-\frac{(n-1)^2}{4N_0^2}\right), \tag{26}$$

where the radius of the nanotube is $R_0=N_0\times a/2$. The boundary conditions in Eq. (25) describe a semi-infinite nanotube attached at position N_0, and also approximate the boundary of a plane at position N.

The Green's function deep inside the nanotube can be calculated analytically,

$$\mathcal{G}_{ii}^{nt}(\epsilon)=\sum_{n=-\infty}^{n=\infty}\frac{1}{\sqrt{\tilde{\epsilon}^2-4\tilde{t}^2}}\theta\left(|\epsilon|-\frac{v_Fn}{R_0}\right). \tag{27}$$

The density of states in the plane has been calculated numerically, with $N=1600$ and summing angular momenta from $n=-100$ to $n=100$. The calculation is equivalent to analyzing a cluster with $(2\times 100+1)\times 1600=321\,600$ sites.

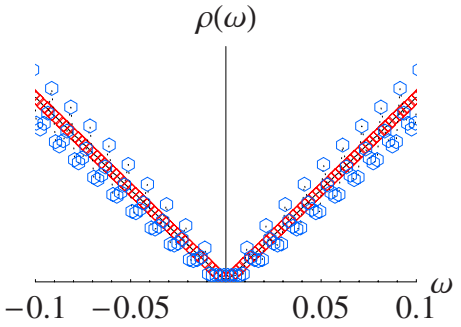

FIG. 6. (Color online) Density of states at the bulk of the nanotube (blue, hexagons), and at the graphene plane (red, diamonds), obtained using the numerical method discussed in the text.

Results for the Green's function in the nanotube, and at the position $i=100$, are shown in Fig. 6. The energy scale is set by $t=1$.

The Green's function for the system built up by the nanotube and the graphene sheet is shown in Fig. 7. The parameters are the same as the ones used for the calculation shown in Fig. 6, and the radius of the nanotube is $N_0=100$.

The density of states at distances from the nanotube $n \gtrsim N_0$ is similar to those in the unperturbed sheet. Near the juncture with the nanotube, there is a depletion of states at low energies, compensated by the existence of a localized state at $\epsilon=0$.

F. Gauge fields due to elastic strains

We have not analyzed so far the effect on the electronic structure of strains which may be induced near the junction. These strains deform the bonds, and induce an additional, intravalley gauge field acting on the electrons.[3,21–23] The large in-plane stiffness of graphene implies that the bonds will tend to their equilibrium lengths throughout the system.

The bending at the junction will be localized within a length scale $l \sim \sqrt{\kappa/\bar{\lambda}}$, where $\kappa \sim 1$ eV is the bending rigidity of graphene, and $\bar{\lambda} \sim 10$ eV Å^{-2} is an average of the Lamé coefficients of graphene. This length is comparable to the lattice spacing.

The mismatch between the diameter of the nanotube and the lattice constant of the graphene layer induces additional strains, with a long-range decay into the bulk of the graphene plane and the nanotube, which can be calculated using the continuum theory of elasticity.[24] We expect, however, the interatomic distance in graphene to be very close to the distance between carbon atoms along the radial direction of the nanotube, so that the strains induced by this effect will be small. The strains will decay as r^{-1} or z^{-1} as function of the distance to the junction.

Using dimensional analysis, the strain near the junction is of order $\Delta R_0/R_0$, where ΔR_0 is the change in the equilibrium radius of the nanotube induced by the plane or, alternatively, of order $\Delta a/a$, where a is the interatomic distance. We expect the value of $\Delta a/a$ to be similar on the plane side of the junction. The associated gauge field is $A \sim \beta \Delta a/a^2$, where $\beta \sim \partial \log(t)/\partial \log(a) \sim 2-3$ gives the change of the tight-binding hopping t with a. Thus, we expect that the elastic strains will induce changes on the electronic structure on energy scales of order $v_F A$ near the junction.

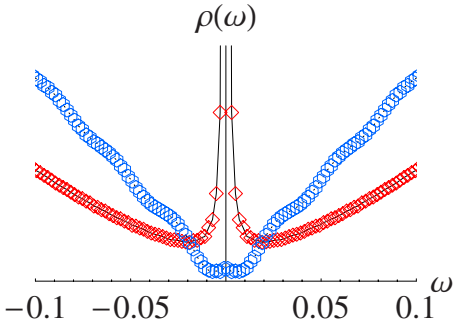

FIG. 7. (Color online) Density of states at a graphene plane attached to a nanotube. The radius of the nanotube is $N_0=100$. The density of states is shown at position $n=10$ from the junction (red, diamonds), and $n=100$ (blue, hexagons).

IV. LOW-ENERGY BANDS IN ARRAYS OF NANOTUBE-GRAPHENE JUNCTIONS

Our computational framework allows us also to address the electronic properties of arrays of nanotube-graphene junctions. We consider the case in which the unit cell of the array has a hexagonal shape in the base, of the type shown in Fig. 1. The periodic arrangement of junctions is formed then by translating the unit cell by two independent vectors of the triangular array, in such a way that the 2D base is fully covered with the hexagonal patches. The Brillouin zone of the superlattice is a hexagon, and the main electronic properties are encoded in the form of the bands from the center to the M and K points at the boundary of the zone. As long as the states in momentum space have well-defined transformation properties under translations by the lattice vectors of the triangular array, we can obtain the bands of the array of junctions by solving a tight-binding model in the unit cell, with appropriate momentum-dependent boundary conditions between opposite sides of its hexagonal base.

The band structure of the array of junctions depends on the geometry of the nanotubes, as well as on their length and the distance between them. For simplicity, we are going to consider arrays where all the nanotubes have the same chirality. Then, it can be checked that the arrays fall into two main classes, regarding the behavior of the bands close to the Fermi level. The distinctive feature of one class with respect to the other is the presence of flat bands in the low-energy part of the spectrum. The arrays of junctions made of armchair nanotubes, for instance, always have a number of these flat bands, as illustrated by the representative in Fig. 8(a). The appearance of flat bands in a particular array of junctions was noticed in Ref. 4. We have found that the flat bands are actually generic in arrays made of armchair nanotubes, which display a series of them as one moves from the Fermi level to higher (or lower) energies. The spacing in energy between the flat bands becomes inversely proportional to the length of the nanotubes. The bands dispersing at low energies in Fig. 8(a) are not affected however by variations in that variable, while they move instead closer to the Fermi

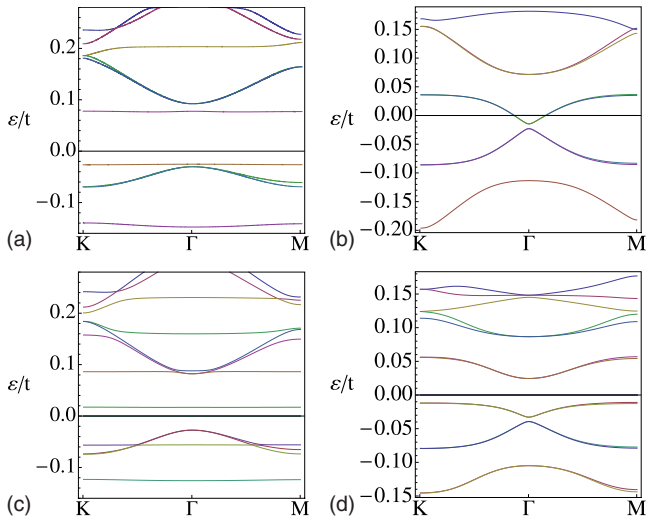

FIG. 8. (Color online) Low-energy bands of arrays of junctions with nanotube geometries (a) (12,12), (b) (12,0), (c) (18,0), and (d) (24,0). In all the cases the unit cell of the array is of the type shown in Fig. 1, with a side of the hexagon in the basal plane equivalent to ten carbon rings of the graphene sheet, and a nanotube height equivalent to ten unit cells of the nanotube for (a), (b), (c), and 20 nanotube unit cells for (d).

level as the distance between the nanotubes in the array is increased.

On the other hand, the presence of flat bands at low energies is not generic in arrays made of zigzag nanotubes. In general, we may expect a number of bands dispersing above and below the Fermi level, as shown in Figs. 8(b) and 8(d), which represent the low-energy bands of arrays made, respectively, of (12,0) and (24,0) nanotubes. In the case of the zigzag nanotubes, flat bands only appear close to the Fermi level when the junctions are formed with $(6n,0)$ geometries such that n is a multiple of 3. This distinctive behavior can be appreciated in Fig. 8(c), which displays the low-energy bands in the case of an array made of (18,0) nanotubes. The shape of the bands resembles there the typical appearance of the spectra of arrays made of armchair nanotubes, as shown in Fig. 8(a).

The mentioned flat bands have their origin in the existence of localized states in the arrays of junctions. We have checked that the junctions made of armchair nanotubes and $(6n,0)$ nanotubes with n equal to a multiple of 3 have in common the formation of electron states confined mostly in the nanotube side. These are the states responsible for the development of the flat bands shown in Fig. 8, as the wave functions with most of their weight in the nanotubes show little overlap in the graphene part of the lattice. This also explains in a natural way the proliferation of flat bands at low energies as the nanotube length is increased, by thinking of the confined modes as standing waves in the tube. On the other hand, the states that are preferentially localized at the junctions (corresponding to the quasibound states of the Dirac equation) may be identified here as the pairs of branches degenerated at the Γ point. These states may have in general a significant overlap between nearest junctions, which is reflected in the appreciable dispersion of the corresponding bands.

We can reach in the continuum limit a qualitative understanding of the similar behavior of the arrays made of armchair and $(6n,0)$ nanotubes when n is a multiple of 3, by noticing that these are the only geometries that support low-energy standing waves between the junction and the other end of the tube. This requires the superposition of two modes with opposite momenta along the tube, which is possible at low energies in the armchair nanotubes as the modes at opposite Dirac points have then vanishing angular momentum. In general, this is not the case for the $(6n,0)$ geometries, since in the zigzag nanotubes the Dirac points correspond to large momenta in the transverse direction. Yet the formation of standing waves is possible when n is a multiple of 3, as the low-energy states about the two Dirac points fall then in the same sector with quantum number $q=1$ regarding the C_{6v} symmetry. Thus, it is possible to form a state confined in the nanotube by superposition of two modes with opposite longitudinal momenta and the same quantum number q. This is consistent with the fact that the confined states are actually found in the $q=1$ sector in the diagonalization of very large lattices of individual nanotube-graphene junctions. In the real lattice of the array, the confinement of the electrons in the nanotubes is only approximate, but the decay of the wave functions in the graphene part away from the junctions is strong enough to account for the development of the flat bands shown above.

V. CONCLUSIONS

In this paper we have studied the electronic structure of the hybrid material made of carbon nanotubes attached to a graphene sheet. By analyzing individual nanotube-graphene junctions, we have found the following features:

(i) Low-energy electrons in the graphene layer, with $|\varepsilon| \lesssim v_F/R_0$, are scattered by the nanotube, and the probability of propagating into the tube is small.

(ii) High-energy electrons reaching the nanotube junction, with $|\varepsilon| \gtrsim v_F/R_0$, are mostly transmitted into the nanotube.

(iii) At low energies, $|\varepsilon| \lesssim v_F/R_0$, and in the vicinity of the junction, $r \sim R_0$, there is in general a depletion of the density of states.

(iv) In certain nanotube geometries [armchair and $(6n,0)$ with n equal to a multiple of 3], there are quasibound states near $\varepsilon=0$, partially localized at the junction.

We have shown that these features can be accounted for in a continuum model of the hybrid geometry. This is based on the Dirac fermion fields describing the electronic excitations, interacting with the curvature and the effective gauge field arising from the six heptagonal carbon rings at the junction. Thus, properties (i), (ii), and (iii) are intrinsic to the continuum Dirac equation and universal for all nanotube geometries, while (iv) depends on the relative position of the six heptagonal rings and the consequent effective magnetic flux at the junction. While we have focused on the case of armchair and zigzag nanotubes, it becomes clear that the continuum theory may account as well for the properties of junctions with other geometries. In this respect, it is likely that, by allowing for less regular distributions of the heptagonal rings, nanotubes with nontrivial helicity can also be attached

to the graphene sheet. In a more general theoretical perspective, it may be interesting to analyze other discrete realizations of the 2D Dirac equation, like the geometry of a square lattice with one half magnetic flux per plaquette.

We have also shown that the arrays of nanotube-graphene junctions fall into two main classes, depending on whether their spectra exhibit or not flat bands close to the Fermi level. The flat bands only appear in arrays made of armchair nanotubes or $(6n,0)$ nanotubes when n is a multiple of 3. On the other hand, the semiconducting behavior seems to be a constant in the class characterized by the presence of the flat bands, as no dispersive bands cross then the Fermi level. Metallic behavior of the array of junctions is possible in the other class, as shown in Fig. 8(b), though that behavior does not appear to be a generic trend, as illustrated by the absence of low-energy bands crossing the Fermi level in the other representative of the class shown in Fig. 8(d).

In real experimental samples, it is quite likely that the arrays may be formed by junctions with nanotubes of different helicities. In this case, we can expect that the electronic structure of these arrays will be a mixture of the features already present in Figs. 8(a)–8(d). In particular, part of the electronic states will be still confined in some of the nanotubes, and other states will be partially localized at some of the junctions. The feasibility of using the arrays of nanotube-graphene junctions may depend on the possibility to tailor these hybrid structures to get specific functions. At this point, more input from experimental measurements on these arrays would be required, while the remarkable behavior predicted for these systems (localization and confinement of states, flat bands) opens good perspectives in the investigation of novel electronic devices.

ACKNOWLEDGMENTS

We acknowledge many helpful discussions with A. H. Castro Neto, who also mentioned to us the existence of Ref. 5. We acknowledge financial support from MEC (Spain) through Grants No. FIS2005-05478-C02-01 and No. FIS2005-05478-C02-02, and CONSOLIDER CSD2007-00010, by the Comunidad de Madrid, through CITECNOMIK, CM2006-S-0505-ESP-0337.

[1] K. S. Novoselov, A. K. Geim, S. V. Morozov, D. Jiang, Y. Zhang, S. V. Dubonos, I. V. Gregorieva, and A. A. Firsov, Science **306**, 666 (2004).
[2] K. S. Novoselov, D. Jiang, F. Schedin, T. J. Booth, V. V. Khotkevich, S. V. Morozov, and A. K. Geim, Proc. Natl. Acad. Sci. U.S.A. **102**, 10451 (2005).
[3] A. H. Castro Neto, F. Guinea, N. M. R. Peres, K. S. Novoselov, and A. K. Geim, Rev. Mod. Phys. **81**, 109 (2009).
[4] T. Matsumoto and S. Saito, J. Phys. Soc. Jpn. **71**, 2765 (2002).
[5] See http://jp.fujitsu.com/group/labs/downloads/en/business/activities/activities-3/fujitsu-labs-nanotech-001-en.pdf.
[6] J. González, F. Guinea, and M. A. H. Vozmediano, Phys. Rev. Lett. **69**, 172 (1992).
[7] J. González, F. Guinea, and M. A. H. Vozmediano, Nucl. Phys. B **406**, 771 (1993).
[8] The value of $\pm 4n$ for the angular momentum is found by noticing that, in the $(6n,0)$ zigzag nanotubes, the Fermi points correspond to large momenta $\pm 4\pi/3\sqrt{3}a$ (a being the C-C distance) for the movement in the direction transverse to the nanotube axis. This leads to a phase of $\pm 8\pi n$ picked up by electrons turning around the nanotube, taking into account the circular length of $6n\sqrt{3}a$ for a $(6n,0)$ geometry.
[9] P. E. Lammert and V. H. Crespi, Phys. Rev. B **69**, 035406 (2004).
[10] N. D. Birrell and P. C. W. Davies, *Quantum Fields in Curved Space* (Cambridge Univ. Press, Cambridge, 1982).
[11] V. M. Pereira, F. Guinea, J. M. B. Lopes dos Santos, N. M. R. Peres, and A. H. Castro Neto, Phys. Rev. Lett. **96**, 036801 (2006).
[12] S.-H. Dong, X.-W. Hou, and Z.-Q. Ma, Phys. Rev. A **58**, 2160 (1998).
[13] M. Büttiker, Phys. Rev. B **32**, 1846 (1985).
[14] M. Hentschel and F. Guinea, Phys. Rev. B **76**, 115407 (2007).
[15] P. M. Ostrovsky, I. V. Gornyi, and A. D. Mirlin, Phys. Rev. B **74**, 235443 (2006).
[16] M. I. Katsnelson and K. S. Novoselov, Solid State Commun. **143**, 3 (2007).
[17] D. S. Novikov, Phys. Rev. B **76**, 245435 (2007).
[18] F. Guinea, J. Low Temp. Phys. **153**, 359 (2008).
[19] M. I. Katsnelson, F. Guinea, and A. K. Geim, arXiv:0901.1398 (unpublished).
[20] B. Wunsch, T. Stauber, and F. Guinea, Phys. Rev. B **77**, 035316 (2008).
[21] S. V. Morozov, K. S. Novoselov, M. I. Katsnelson, F. Schedin, L. A. Ponomarenko, D. Jiang, and A. K. Geim, Phys. Rev. Lett. **97**, 016801 (2006).
[22] J. L. Mañes, Phys. Rev. B **76**, 045430 (2007).
[23] F. Guinea, M. I. Katsnelson, and M. A. H. Vozmediano, Phys. Rev. B **77**, 075422 (2008); F. Guinea, B. Horovitz, and P. Le Doussal, *ibid.* **77**, 205421 (2008).
[24] L. D. Landau and E. M. Lifschitz, *Theory of Elasticity* (Pergamon Press, Oxford, 1959).